A two-dimensional statistical framework connecting thermodynamic profiles with filaments in the scrape off layer and application to experiments

Cite as: Phys. Plasmas **25**, 056112 (2018); https://doi.org/10.1063/1.5017919
Submitted: 01 December 2017 . Accepted: 04 March 2018 . Published Online: 09 May 2018

F. Militello, T. Farley, K. Mukhi, N. Walkden, and J. T. Omotani

A two-dimensional statistical framework connecting thermodynamic profiles with filaments in the scrape off layer and application to experiments

F. Militello,[1,a)] T. Farley,[1,2] K. Mukhi,[1,3] N. Walkden,[1] and J. T. Omotani[1]
[1]*CCFE, Culham Science Centre, Abingdon, Oxon OX14 3DB, United Kingdom*
[2]*Department of Electrical Engineering and Electronics, University of Liverpool, Brownlow Hill, Liverpool L69 3GJ, United Kingdom*
[3]*School of Physics and Astronomy, University of Manchester, Oxford Road, Manchester M13 9PL, United Kingdom*

(Received 1 December 2017; accepted 4 March 2018; published online 9 May 2018)

A statistical framework was introduced in Militello and Omotani [Nucl. Fusion **56**, 104004 (2016)] to correlate the dynamics and statistics of L-mode and inter-ELM plasma filaments with the radial profiles of thermodynamic quantities they generate in the Scrape Off Layer. This paper extends the framework to cases in which the filaments are emitted from the separatrix at different toroidal positions and with a finite toroidal velocity. It is found that the toroidal velocity does not affect the profiles, while the toroidal distribution of filament emission renormalises the waiting time between two events. Experimental data collected by visual camera imaging are used to evaluate the statistics of the fluctuations, to inform the choice of the probability distribution functions used in the application of the framework. It is found that the toroidal separation of the filaments is exponentially distributed, thus suggesting the lack of a toroidal modal structure. Finally, using these measurements, the framework is applied to an experimental case and good agreement is found.
https://doi.org/10.1063/1.5017919

I. INTRODUCTION

Density and temperature profiles in the boundary region of magnetic fusion devices determine the average interaction between the plasma and the plasma facing components, thus controlling the amount of erosion they are subject to, and therefore their lifetime. In addition, fueling efficiency and optimised coupling of resonant frequency heating schemes require an accurate tailoring of the density profile. It is well known that plasma fluctuations in the Scrape Off Layer (SOL), i.e., the external region of the plasma in magnetic contact with solid surfaces, are particularly large.[1,2] These density and temperature perturbations, called filaments after their elongation along the magnetic field, can deposit transient and intermittent loads on the walls of the machine and induce fatigue effects.

In Refs. 3 and 4, we introduced a statistical framework based on the independent and uniform emission of L-mode and inter-ELM filaments in order to correlate their dynamics with the SOL profiles they generate (i.e., their average effect). This approach was inspired by a seminal paper by Garcia[5] which treated the filaments as a Poisson process in order to obtain point-wise features of the turbulence statistics (e.g., the probability distribution function of the fluctuations, its statistical moments, the power spectrum). Our treatment extended the calculation by correlating different points in the SOL through the definition of the radial and parallel dynamics of the filaments, and thus obtaining radial profiles of thermodynamic quantities rather than just point-wise estimates. Both the point-wise treatment[6,7] and our own[8] have proved to be effective in matching experimental measurements in various machines.

The aim of the present paper is to further extend our framework by allowing for new and more realistic conditions for the filament motion, in particular we will introduce the effect of a finite toroidal velocity. Also, we will compare the results of the framework with experimental data obtained with a visual camera system in MAST.

II. DERIVATION OF THE FRAMEWORK

Our framework is based on a Lagrangian approach to filament dynamics, where each filament has its own motion and its parallel and perpendicular dynamics are treated separately.[3,4] Importantly, the perturbations are assumed not to interact with each other and to be uniformly emitted from the core. This hypothesis was explored in Ref. 9 and makes SOL filaments alike raindrops from a statistical viewpoint. Using a Lagrangian approach, the generic thermodynamic quantity, η, transported by an individual filament labelled i is given by

$$\eta_i(x,y,t) = \eta_{0,i} F_i(t) \Lambda\left(x - \int_0^t V_{x,i}(t')dt', y - y_0 - \int_0^t V_{y,i}(t')dt', w_{x,i}, w_{y,i}\right). \quad (1)$$

Here η represents a generic field, e.g., the density or the temperature in the filament, while η_0 is the initial amplitude as the perturbation crosses the separatrix. We assume that "radial" and "toroidal" coordinates are defined by $x = R - R_{sep}$ and $y = R\phi$, respectively, where R is the major radius of the machine and ϕ the toroidal angle. Here, $x = 0$ gives the position

Note: Paper YI2 4, Bull. Am. Phys. Soc. **62**, 403 (2017).
[a)]Invited speaker.

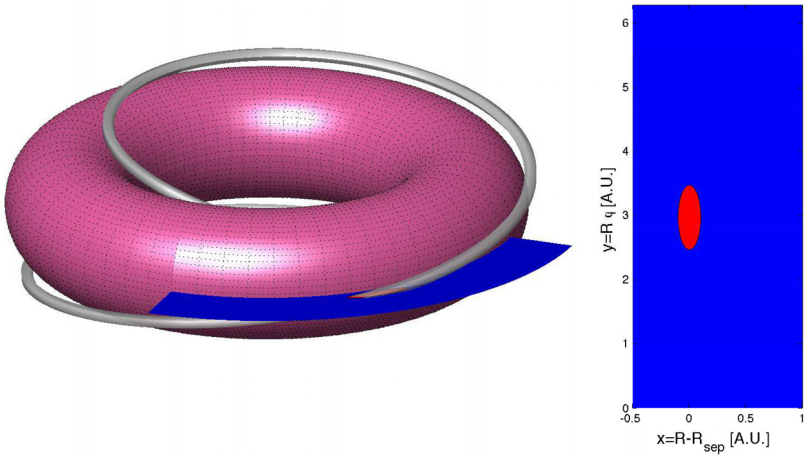

FIG. 1. Schematic representation of the geometry of the problem. Left: Using a toroidal plasma configuration as a reference (pink), the dynamics of a filament (gray) are followed in a toroidal plane (blue). Note that the filament is open and, in this configuration, it would terminate on the high field side limiter (not shown). The red ellipse represents the intersection between the plane and the filament and its evolution is described by the equations in the main text. Right: toroidal plane of interest straightened and, in the configuration, used by the statistical model.

of the separatrix and $y = y_0$ is the toroidal position where the filament crosses the separatrix. One could imagine the x–y plane to be a toroidal plane (e.g., the mid-plane) on the low field side of the device, but it does not need to be restricted to that. Figure 1 gives an idea of the system of coordinates and how a filament would look like if projected on it. The filament propagates in the radial direction with a velocity V_x and in the toroidal with a velocity V_y. These velocities can depend on time, space or filament parameters, such as their radial or toroidal widths, w_x and w_y. In other words, at this stage, the velocities are generic functions. Similarly, the functional form of the draining function F also does not need to be specified yet. F represents the fact that the perturbed thermodynamic quantities are transported outside the x–y plane along the field lines and towards the plasma facing components. Finally, Λ is a generic function representing the shape of the cross-section of the filament in the x–y plane. A schematic representation of the dynamics of an isolated filament is given in the left panel of Fig. 2.

Note that the helical symmetry of the filaments implies that their toroidal and poloidal motions are interchangeable and indistinguishable due to the so-called barber pole effect. As a consequence, as far as the statistical framework is concerned, the toroidal velocity discussed here could be caused, partially or entirely, by a poloidal rotation of the filament. Geometric projections would then allow to easily turn the poloidal motion into toroidal (and vice-versa).

Implicitly, we assume that a large number of filaments contribute to the generation of the SOL profiles and each of them has different characteristics (width, initial amplitude,…), drawn from appropriate statistical distributions. In principle, these characteristics determine the evolution and the draining of the filament, i.e., the F and V functions are governed by a so far unspecified law which is identical for all filaments but can depend on their features (w_i, η_i,…).

The next step is to build synthetic 2D SOL configurations based on the superposition of many filamentary events. This can be easily done by writing

$$\theta(x, y, t) = \sum_{i=1}^{K} \eta_i(x, y, t - t_{0,i}), \tag{2}$$

where $\theta(x, y, t)$ represents an instantaneous snapshot of the density in the midplane. Here, we have K filaments in a period of time ΔT and the emission of the ith filament from the separatrix occurs at the time $t = t_{0,i}$. For a given x and y, the signal produced by Eq. (2) is also known as shot noise and it has the features of a Poisson process[5,10] if the $t_{0,i}$ are uniformly distributed. An example of an instantaneous synthetic realisation for a thermodynamic quantity in the SOL is given in the right panel of Fig. 2.

We are now ready to evaluate the SOL profiles at a given toroidal position, $y = y_*$, similarly to what is done

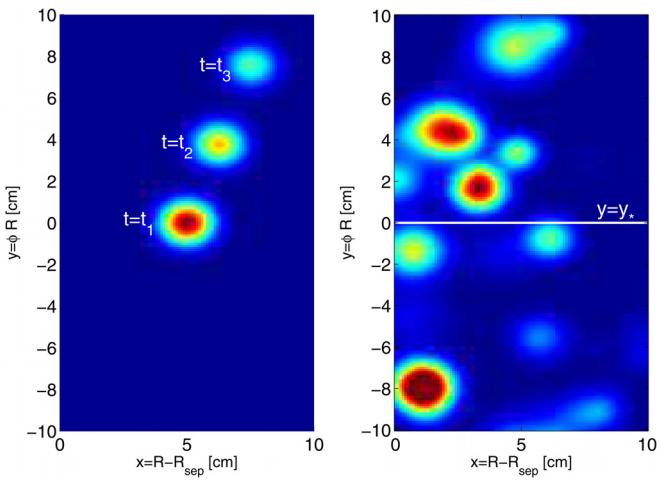

FIG. 2. Left: Isolated filament with a Gaussian cross-section evolving with a radial and toroidal velocity and fading due to draining in the parallel direction. The figure shows the evolution at three different times: t_1, t_2 and t_3. Right: instantaneous realisation of the field of interest (e.g., density, temperature,…) produced by the combination of several independent filaments with statistically distributed amplitudes, widths and the initial position at the separatrix. A solid line in the center of the plot shows the (arbitrary) toroidal location where we evaluate the profiles. The figure is a sketch aimed at showing the typical behaviour of the filaments in the framework and is not associated with any particular physical realisation.

experimentally when plunging a reciprocating probe in the boundary plasma. The average over time of the synthetic signal is given by

$$\Theta_{\Delta T}(x) = \frac{1}{\Delta T}\int_0^{\Delta T} dt \sum_{i=1}^{K} \eta_i(x, y_*, t - t_{0,i}). \tag{3}$$

In typical conditions, the average is done over a time period ΔT much larger than the time scale associated with a single filament. Also, the number of filaments K is a statistical quantity which is Poisson distributed due to the way we constructed our problem.

At this point, we have two possible ways forward. The first is to produce a time evolving synthetic field using Eq. (2) with filaments sampled from given distributions and with the dynamics regulated by V_x, V_y and F and then perform the time average Eq. (3). This can be easily done with simple numerical codes and Fig. 2 was produced using this technique. The second approach leads to further analytical progress in the limit $\Delta T \to \infty$. Due to the statistical nature of the process and the fact that it is ergodic by construction,[10] we can replace the time averages with ensemble averages, so that we can abstract the problem and avoid being tied to a specific realisation of the system. In the rest of the paper, we follow this second approach, which leads to

$$\Theta_{\Delta T}(x) = \int_0^{\infty} d\eta_0 P_{\eta_0} \int_0^{\infty} dw P_w \int_{y_{min}}^{y_{max}} dy_0 P_{y_0} \times \sum_{K=1}^{\infty} P_K \sum_{j=1}^{K} \int_0^{\Delta T} dt_0 P_{t_0} \eta(x, y_*, t - t_{0,j}). \tag{4}$$

Here, the subscript i was dropped because the description of the individual filaments is replaced by their statistical properties defined by P_{η_0}, P_{y_0} and P_w, which are the so far undefined probability distribution functions (PDFs) of the initial amplitudes, toroidal positions and widths, respectively. In addition, $P_K = \lambda^K e^{-\lambda}/K!$ is the Poisson distribution representing the probability that K filaments are emitted over a period ΔT, $\lambda = \Delta T/\tau_w$ with τ_w being the average time between filaments, i.e., their waiting time (inverse of the emission rate or rate of the Poisson process) and $P_{t_0} = 1/\Delta T$ is the homogeneous probability distribution of the arrival times associated with a Poisson process. The integration over the initial toroidal position is performed between a minimum and a maximum value, y_{min} and y_{max}. To write Eq. (4) in a compact form, we took $w_x = w_y = w$, but this is not a necessary assumption and this simplification can be easily removed. Note that the dependence on t on the right hand side of Eq. (4) is only apparent (no time dependence is present on the left hand side of the same equation). This can be explained using Campbell's theorem for shot noise,[10] which allows us to write

$$\lim_{\Delta T\to\infty} \sum_{K=1}^{\infty} P_K \sum_{j=1}^{K} \int_0^{\Delta T} dt_0 P_{t_0} \eta(x, y_*, t - t_{0,j}) = \frac{1}{\tau_w}\int_{-\infty}^{\infty} dt \eta(x, y_*, t). \tag{5}$$

From the right hand side of this equation, we can see that the explicit time dependence disappears.

The final step is to calculate from Eq. (4) the average profiles in the limit $\Delta T \to \infty$

$$\Theta(x) = \{\eta(x, y_*, t)\} = \frac{1}{\tau_w}\int_{-\infty}^{\infty} dy_0 \int_{-\infty}^{\infty} dt \int_0^{\infty} d\eta_0 \times \int_0^{\infty} dw \left[\eta(x, y_*, t) P_{\eta_0}(\eta_0) P_w(w) P_{y_0}(y_0)\right], \tag{6}$$

where we used curly brackets to define the ensemble average operator. Note that typically we imagine a system that is periodic in the y direction (i.e., the toroidal direction). Taking this into account, the integral over y_0 can be expressed as $\sum_{k=-\infty}^{\infty} \int_{2\pi R(k-1)}^{2\pi Rk} dy_0 P_{y_0} = \int_{-\infty}^{\infty} dy_0 P_{y_0}$.

The procedure discussed so far for the average profiles can be straightforwardly applied to other statistical properties of the signal, such as the variance, $\sigma(x)^2 = \{\eta(x, y_*, t)^2\}$, the skewness, $S = \{\eta(x, y_*, t)^3\}/\{\eta(x, y_*, t)^2\}^{3/2}$, and the kurtosis, $K = \{\eta(x, y_*, t)^4\}/\{\eta(x, y_*, t)^2\}^2$ (to avoid confusion, note that Refs. 3 and 4 use two different notations for the variance and the one that we use here is consistent with Ref. 4).

Equation (6) together with the expressions for σ^2, S and K form the final result of the statistical framework as they correlate the statistical (P_w, P_{η_0}, P_{y_0}) and dynamical (V_x, V_y, F) properties of the filaments with the average profiles (Θ) and the macroscopic statistical properties of the turbulence (σ, S, K,…), as experimentally measured. In principle, the radial behaviour of the full probability distribution function of the turbulent fluctuations could be obtained, as well as correlation functions, energy spectra and other statistical properties. These derivations for point-wise measurements are presented in Refs. 5 and 11, and our framework, being an extension of the point-wise model, inherits all its properties.

The strength of the statistical framework presented here is its flexibility. Indeed, both the PDFs of the filaments, P_{y_0}, P_w and P_{η_0} and the function describing their motion, V_x, V_y and F, are generic and can be user-defined. As a consequence, theoretical models, fit to experimental measurements or a combination of the two are suitable for use in the framework. In Sec. IV, a particular choice of the statistics and dynamics of the filaments will be considered in order to elucidate how the framework is applied and to shed some light on how filament parameters affect the profiles.

III. PARAMETERISATION OF THE CROSS FIELD TRANSPORT

An approach often used in the analysis of experimental measurements and in multi-fluid calculations is to parameterise the SOL cross field transport using an effective diffusion coefficient or an effective velocity. In other words, the average radial flux is linearly related to the thermodynamic quantity and its gradient

$$\Gamma(x) = V_{eff}\Theta(x) + D_{eff} d\Theta(x)/dx. \tag{7}$$

Experimentally[12,13] and numerically,[13–15] it was shown that this diffusive-advective approach, while widely used, gives a

poor parameterisation of the data in the SOL, at least for the density. This is not surprising, considering that the amplitude of the (density) fluctuations in the SOL is comparable with their time average,[16,17,20] and under these conditions, the diffusive-advective paradigm cannot be justified.

The statistical framework presented here provides an alternative way for capturing the profile formation and its parametrisation. It suggests that the fluctuations should be experimentally characterised and, through the framework, used to interpret measurements and extrapolate to new devices (i.e., scaling laws for D_{eff} and V_{eff} should be replaced by scaling laws for the PDFs and the dynamics of the fluctuations). However, to connect with earlier results, it is useful to derive transport coefficients from the statistical model. This can be easily done by calculating the radial flux, which is given by

$$\begin{aligned}\Gamma(x) &= \{\eta(x,y_*,t)V_x\} \\ &= \frac{1}{\tau_w}\int_{-\infty}^{\infty} dy_0 \int_{-\infty}^{\infty} dt \int_0^{\infty} d\eta_0 \\ &\quad \times \int_0^{\infty} dw \left[V_x \eta(x,y_*,t) P_{\eta_0}(\eta_0) P_w(w) P_{y_0}(y_0)\right]. \end{aligned} \quad (8)$$

Using Eqs. (6)–(8), it is easy to determine D_{eff} and V_{eff}.

IV. EXAMPLE OF A SIMPLE APPLICATION

In order to gain some insight into the effect of a random toroidal emission and a toroidal velocity of the filaments, we apply the statistical framework to a simple case. We assume that all the filaments have the same initial amplitude and width (corresponding to delta function PDFs) that their radial and toroidal velocities are constant and that their draining function is represented by a decaying exponential with a constant decay time. In addition, the filaments are emitted from the separatrix in random toroidal positions in a uniform way. From a mathematical point of view, we have that: $P_{y_0} = 1/(2\pi R)$, $P_w = \delta(w - w_*)$, $P_{\eta_0} = \delta(\eta_0 - \eta_*)$, $V_x = const$, $V_y = const$, $F = e^{-t/\tau}$. We compare two different filament shapes, both with a Gaussian behaviour in y, one with a truncated exponential in x: $\Lambda = e^{-y^2/w_y^2} e^{x/w_x} H(-x)$ and one Gaussian in x: $\Lambda = e^{-x^2/w_x^2 - y^2/w_y^2}$. The former case would represent a filament that produces a steep front as it propagates,[18,19] while the second would be more relevant under dissipative conditions, where collisional transport homogenises the filament.[20,21]

With straightforward algebra, we find that

$$\Theta(x) = \frac{\sqrt{\pi} w_y}{2\pi R} \frac{\eta_*}{\frac{\tau_w}{\tau}} G\left(2\frac{V_x \tau}{w_x}\right) e^{-\frac{x}{V_x \tau}}, \quad (9)$$

where $G(\alpha) = 1/(1+\alpha/2)$ for the truncated exponential case, and $G(\alpha) = e^{1/\alpha^2} Erfc(1/\alpha)/\alpha$ for the double Gaussian shape (here, *Erfc* is the complementary error function). By comparing these two expressions, one notices that the shape of the filament has a minor effect on the radial profile, only slightly changing the functional dependence of the separatrix value of the profile on $V_x\tau/w_x$. The ratio of the two expressions for $G(\alpha)$ is close to $\sqrt{\pi}$ for all α, corresponding to the ratio of the integrals over x and y of the two expressions for Λ.

It is worth noticing that Eq. (9) does not have an explicit dependence on the toroidal velocity V_y, which is a natural consequence of the assumption of toroidal symmetry and is therefore a general result. The factor $\frac{\sqrt{\pi} w_y}{2\pi R}$ can be seen as a renormalisation of the waiting time τ_w. Indeed, τ_w is the waiting time for a filament to appear at the separatrix *in a random toroidal position*, while $\tau_w' \equiv \tau_w\left(\frac{2\pi R}{\sqrt{\pi} w_y}\right)$ is the waiting time for a filament to appear *at a given toroidal angle*, equivalent to the waiting time in the 1D model developed in Refs. 3 and 4. In the limits $P_{y_0} = \delta(y_0 - y_*)$ and $V_y = 0$, Eq. (9) would correctly reduce to Eq. (9) of Ref. 3 and Eq. (15) of Ref. 4, derived for a single toroidal position and no toroidal velocity.

While the toroidal velocity does not affect the shape of the profiles, it can modify other statistical properties of the turbulence. For example, the autocorrelation time in a Langmuir probe-like analysis would tend to shorten as the velocity increases. In general, anything not toroidally averaged or time averaged could be affected.

Finally, as already noticed in Refs. 3 and 4, an exponentially decaying profile is typically not a satisfactory representation of the experimental profiles in most cases (but not all, as shown in Sec. V), which tend to have an increasing decay length as one moves towards the far SOL. The case treated here was simplified on purpose to allow a closed analytical form and would need more sophistication to treat flattened and broadened profiles (e.g., radially varying V and F, as discussed in Ref. 8). Equation (9), however, qualitatively describes the main dependencies of the profile on the filament features.

V. EXPERIMENTAL OBSERVATIONS AND COMPARISON

In Sec. IV, we assumed that the emission of the filaments from the separatrix is uniform at toroidal angles. This is equivalent to stating that the plasma eruptions in the SOL are random uncorrelated events generated by a Poisson process. In other words, there is no underlying toroidal modal structure associated with the filaments and no regularity. If this was the case, we would expect the statistical distribution of the toroidal separation between one eruption and the next to be governed by an exponential law. This is no different from the fact that random independent events emitted at a constant rate have an exponential distribution of waiting times.

In order to test this hypothesis, we analysed wide-angle unfiltered visual camera images of MAST, which measure the D_α light emitted by the interaction between the plasma filaments and the neutrals in the SOL at a frame rate of 100 kHz.[22–25] The raw images were pseudo-inverted using a new tomographic reconstruction technique based on the alignment of the filaments with the magnetic field (reconstructed with the EFIT code). A grid of field lines, uniformly launched at given radial and toroidal positions, is projected onto the camera images and the intensity distribution along them is integrated to produce a 2D map of emission in the

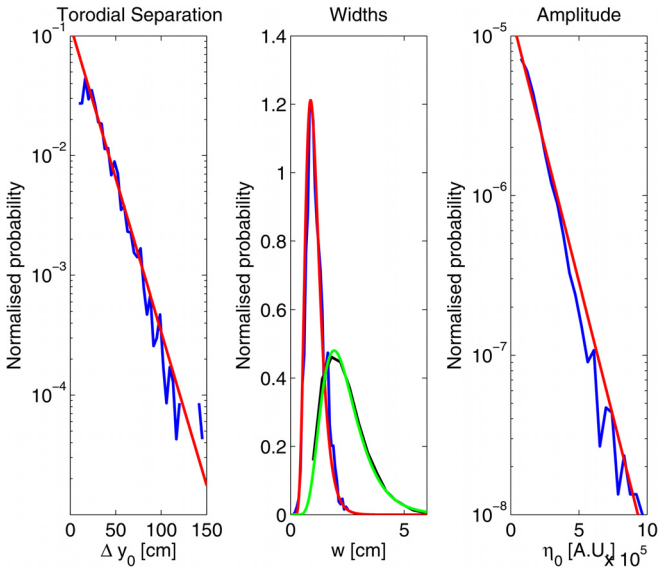

FIG. 3. PDFs of the toroidal separation (left), radial and toroidal widths (center) and amplitude (right) of the filaments. The blue curves are the experimental measurements and the red curves are the analytic fits given in the text (the only exception is the toroidal width PDF, which is black and green, respectively). All data are calculated at the separatrix (R_{sep} = 1.366 m) for MAST discharge 29 852.

SOL. Peaks in the field line emission are then identified in the 2D map and ellipses are fitted to them, returning the filaments' radial and toroidal positions and widths and field line integrated amplitudes. The details of the technique, which are beyond the scope of the present paper, will be the subject of a different publication[26] and are briefly introduced in Ref. 21. For this analysis, we used MAST discharge 29 852, which was previously examined in Refs. 21 and 25. The plasma was in a connected double configuration, in an NBI heated L-mode with a long flat top, with a plasma current of 600 kA, a line average density of around $2 \times 10^{19} \mathrm{m}^{-3}$ in the period examined and a magnetic field on an axis of $0.27T$ ($B_T = 0.4$ at the reference point $R = 0.66$ cm). Similar discharges were also thoroughly discussed in Ref. 27, where typical SOL regimes and filament dynamics for MAST were investigated.

The result of our analysis shows that the toroidal separation of the filaments at the separatrix has indeed an exponential distribution with an average separation of ∼17 cm, see the left panel of Fig. 3. This is consistent with the assumption of independence of the filaments and with the statistical framework. The toroidal separations were measured by determining the instantaneous toroidal profile of the light intensity (roughly proportional to the plasma density) at the separatrix in each frame of the video and by calculating the distance between two successive maxima.

Similarly, we measured the PDFs of the widths and amplitudes of the filaments at the separatrix, finding that the former can be approximated with log-normal distributions and the latter with an exponential distribution, see Fig. 3. In particular, fits to the distributions gave the following expressions $P_{w_x} = \frac{1}{0.35\sqrt{2\pi}w_x} e^{\frac{-\log(w_x)^2}{2\cdot 0.35^2}}$, $P_{w_y} = \frac{1}{0.4\sqrt{2\pi}w_y} e^{\frac{-(\log(w_y)-0.81)^2}{2\cdot 0.4^2}}$ and $P_{\eta_0} = e^{-\eta_0/(1.28\times 10^5)}/(1.28 \times 10^5)$ (note that the amplitude is expressed in arbitrary units due to uncalibrated measurements and the PDF is given only to show the correct functional dependence). The PDFs are well converged and were obtained using a total of more than one thousand events. We used these data in the statistical framework, together with the assumption that $V_x \approx 0.6\,\mathrm{km/s}$ is a constant[21,25] and that the draining is an exponential with decay time given by $\tau = L_{//}/c_s \approx 100$ ms, i.e., the parallel transit time ($L_{//}$ and c_s are the connection length and the sound speed, respectively).

In Fig. 4, we show the comparison between the light intensity profile (representative of the plasma density) and the profile of its variance, both in arbitrary units. Here, we used $R = R_{sep} = 1.366$ m, and the waiting time was a free parameter as it could not be precisely measured experimentally due to the relatively coarse time resolution of the camera. There is quantitative agreement between both profiles and the predictions of the statistical framework if we take $\tau_w \approx 0.4\,\mu$s. This number is reasonable as we see on average around 40 filaments in each camera frame[25] and we estimate that each filament lifetime is around 20–50 μs.[21]

VI. SUMMARY AND CONCLUSIONS

In this paper, we extended the statistical framework introduced in Refs. 3 and 4 to include the effect of a toroidal distribution and a toroidal motion of the SOL filaments. Our

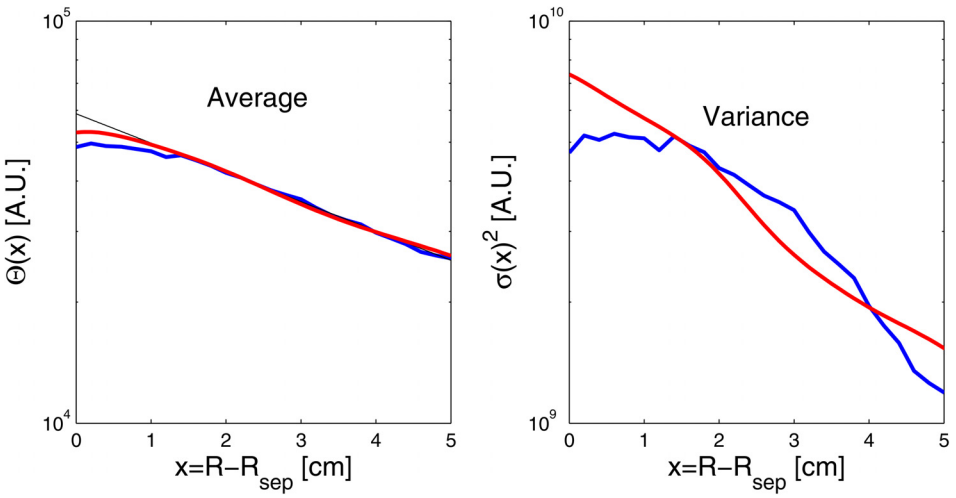

FIG. 4. Comparison between experimental profiles of the intensity of the field line integrated light emission (blue) and the predictions of the statistical framework (red). The profiles of the average and variance are given in the left and right panels, respectively. In the left panel, we fitted the data with an exponential curve, corresponding to a decay length of around 6 cm.

results show that the toroidal velocity does not affect the profiles as long as axisymmetry is assumed. The fact that filaments are emitted at different toroidal locations gives a renormalisation of the average waiting time with respect to the original papers. Measurements of the toroidal separation of the filaments in MAST showed an exponential distribution, which is expected from a Poisson process. Hence, we deduce that the filaments are randomly emitted from the core, in a toroidally uniform way along the separatrix in the midplane region and without a clear modal structure. This reinforces the idea that filaments do behave independently, a hypothesis at the basis of the statistical framework derivation.

Using MAST visual camera data, we compared experimental measurements with the results from the statistical framework, finding good agreement for both the average radial profile and for the variance, simultaneously. This confirms the ability of the framework to capture the behaviour of experimental data in a second machine, after the success of the application to JET data.[8]

In order to connect to previous work in the literature, we also derived the expression for the radial particle flux, which can allow us to estimate the effective transport coefficients. However, the methodology introduced in this paper suggests that, when interpreting and extrapolating, a better way to proceed is to characterise the fluctuations rather than the transport coefficients. This could provide a more first principles approach to SOL transport and allow more reliable predictions for future machines, both in terms of average and intermittent loads. Our work, hopefully, will provide motivation to further experimental and theoretical understanding and characterisation of SOL filament dynamics and statistics.

ACKNOWLEDGMENTS

We thank Dr. C. Ham for carefully reading the manuscript. This work was funded by the RCUK Energy Programme [Grant No. EP/P012450/1]. To obtain further information on the data and models underlying this paper, whose release may be subject to commercial restrictions, please contact PublicationsManager@ukaea.uk.

[1]G. Y. Antar, S. I. Krasheninnikov, P. Devynck, R. P. Doerner, E. M. Hollmann, J. A. Boedo, S. C. Luckhardt, and R. W. Conn, Phys. Rev. Lett. **87**, 065001-1 (2001).
[2]D. A. DIppolito, J. R. Myra, and S. J. Zweben, Phys. Plasmas **18**, 060501 (2011).
[3]F. Militello and J. T. Omotani, Nucl. Fusion **56**, 104004 (2016).
[4]F. Militello and J. T. Omotani, Plasma Phys. Controlled Fusion **58**, 125004 (2016).
[5]O. E. Garcia, Phys. Rev. Lett. **108**, 265001 (2012).
[6]A. Theodorsen, O. E. Garcia, J. Horacek, R. Kube, and R. A. Pitts, Plasma Phys. Controlled Fusion **58**, 044006 (2016).
[7]O. E. Garcia, R. Kube, A. Theodorsen, J.-G. Bak, S.-H. Hong, H.-S. Kim, the KSTAR Project Team, and R. A. Pitts, Nucl. Mater. Energy **12**, 36 (2017).
[8]N. R. Walkden, A. Wynn, F. Militello, B. Lipschultz, G. Matthews, C. Guillemaut, J. Harrison, and D. Moulton, and JET Contributors, Plasma Phys. Controlled Fusion **59**, 085009 (2017).
[9]F. Militello, B. Dudson, L. Easy, A. Kirk, and P. Naylor, Plasma Phys. Controlled Fusion **59**, 125013 (2017).
[10]H. L. Pécseli, *Fluctuations in Physical Systems* (Cambridge University Press, Cambridge, England, 2000).
[11]O. E. Garcia, R. Kube, A. Theodorsen, and H. L. Pecseli, Phys. Plasmas **23**, 052308 (2016).
[12]B. LaBombard, M. V. Umansky, R. L. Boivin, J. A. Goetz, J. Hughes, B. Lipschultz, D. Mossessian, C. S. Pitcher, and J. L. Terry, Nucl. Fusion **40**, 2041 (2000).
[13]O. E. Garcia, R. A. Pitts, J. Horacek, A. H. Nielsen, W. Fundamenski, J. P. Graves, V. Naulin, and J. Juul Rasmussen, J. Nucl. Mater. **363365**, 575–580 (2007).
[14]V. Naulin, J. Nucl. Mater. **363–365**, 24 (2007).
[15]F. Militello, W. Fundamenski, V. Naulin, and A. J. Nielsen, J. Nucl. Mater. **438**, S530 (2013).
[16]B. LaBombard, R. L. Boivin, M. Greenwald, J. Hughes, B. Lipschultz, D. Mossessian, C. S. Pitcher, J. L. Terry, and S. J. Zweben, Phys. Plasmas **8**, 2107 (2001).
[17]J. P. Graves, J. Horacek, R. A. Pitts, and K. I. Hopcraft, Plasma Phys. Controlled Fusion **47**, L1 (2005).
[18]O. E. Garcia, N. H. Bian, and W. Fundamenski, Phys. Plasmas **13**, 082309 (2006).
[19]O. E. Garcia, J. Horaceck, and R. A. Pitts, Nucl. Fusion **55**, 062002 (2015).
[20]F. Militello, P. Tamain, W. Fundamenski, A. Kirk, V. Naulin, and A. H. Nielsen, Plasma Phys. Controlled Fusion **55**, 025005 (2013).
[21]F. Militello, N. R. Walkden, T. Farley, W. A. Gracias, J. Olsen, F. Riva, L. Easy, N. Fedorczak, I. Lupelli, J. Madsen, A. H. Nielsen, P. Ricci, P. Tamain, and J. Young, Plasma Phys. Controlled Fusion **58**, 105002 (2016).
[22]A. Kirk, N. Ben Ayed, G. Counsell, B. Dudson, T. Eich, A. Herrmann, B. Koch, R. Martin, A. Meakins, S. Saarelma, R. Scannell, S. Tallents, M. Walsh, and H. R. Wilson, Plasma Phys. Controlled Fusion **48**, B433 (2006).
[23]B. D. Dudson, N. Ben Ayed, A. Kirk, H. R. Wilson, G. Counsell, X. Xu, M. Umansky, P. B. Snyder, and B. LLoyd, Plasma Phys. Controlled Fusion **50**, 124012 (2008).
[24]N. Ben Ayed, A. Kirk, B. Dudson, S. Tallents, R. G. L. Vann, and H. R. Wilson, Plasma Phys. Controlled Fusion **51**, 035016 (2009).
[25]A. Kirk, A. J. Thornton, J. R. Harrison, F. Militello, and N. R. Walkden, Plasma Phys. Controlled Fusion **58**, 085008 (2016).
[26]T. Farley, N. R. Walkden, and F. Militello, "Filament identification in wide-angle high speed imaging of the Mega Amp Spherical Tokamak" (unpublished).
[27]F. Militello, L. Garzotti, J. Harrison, J. T. Omotani, R. Scannell, S. Allan, A. Kirk, I. Lupelli, and A. J. Thornton, Nucl. Fusion **56**, 016006 (2016).